Structures, Interactions, and Ferromagnetism of Fe–Carbon Nanotube Systems

ARTICLE *in* THE JOURNAL OF PHYSICAL CHEMISTRY C · MAY 2008

Impact Factor: 4.77 · DOI: 10.1021/jp0761968

4 AUTHORS, INCLUDING:

Trinh Vo
NASA
35 PUBLICATIONS **339** CITATIONS

SEE PROFILE

Structures, Interactions, and Ferromagnetism of Fe−Carbon Nanotube Systems

Trinh Vo,[†] Yu-Dong Wu,[‡] Roberto Car,[‡] and Marc Robert*[,†,§,||]

Department of Chemical and Biomolecular Engineering, Rice University, Houston, Texas 77005, Chemistry Department and The Princeton Institute for the Science and Technology of Materials (PRISM), Princeton University, Princeton, New Jersey 08544, Rice Quantum Institute, Rice University, Houston, Texas 77005, and The Richard E. Smalley Institute for Nanoscale Science and Technology, Rice University, Houston, Texas 77005

Received: August 2, 2007; Revised Manuscript Received: February 29, 2008

The structures, interaction, and magnetic properties of Fe atoms with a single-wall carbon nanotube are investigated using Car−Parrinello molecular dynamics. The stability, band gap, Fermi energy, and total magnetic moment of the Fe-adsorbed single-wall carbon nanotube systems are found to depend on the location of the Fe atoms relative to the carbon nanotube surface. The confinement and the curvature of nanotubes have a strong effect on the relative stability of various structures corresponding to different positions of the Fe atom inside and outside carbon nanotubes. The Fe atoms inside a carbon nanotube are found to couple ferromagnetically.

Introduction

Carbon nanotubes (CNs), while simple in structure, have many attractive properties: they are ultrastrong, chemically inert, mechanically flexible, and have diverse electronic and transport properties (they can be metallic or semiconducting, depending on their diameter and chirality). Consequently, CNs are promising candidates for several technical applications[1] ranging from composites,[2] photonics,[3] and quantum dots[4] to nanoelectronic devices such as field-effect transistors[5] and spintronics.[6] In such applications, CNs are usually used either by themselves as constructing building blocks for the devices or in combination with other elements.

CNs are themselves diamagnetic materials. In view of their remarkable properties mentioned above, it would be of interest to make CNs ferromagnetic to further extend their applications.[7] Possible applications of ferromagnetic materials include magnetic recording media devices and spintronic devices. One of the proposed routes to make new magnetic materials based on CNs is to couple single-wall carbon nanotubes (CN) with magnetic transition or rare-earth metals.[7] Before attaining this goal, the study of the physical as well as of the electronic and magnetic properties of transition metal atoms adsorbed on a CN is of current interest from both fundamental and practical points of view. First, knowing the electronic structures and metal-tube interaction of a system of CNs filled with magnetic transition metals is very helpful in studying magnetic properties in low dimensions. Second, since magnetic transition metals (such as Fe, Co, Ni) are used as catalysts in the preparation of CNs,[8] the key role of transition metals in the synthesis of carbon nanotubes should be understood. Furthermore, in nanoelectronic applications, understanding the interaction between the metals and CNs also plays an important role in making devices having low resistance contact between metals and CNs as well as in other issues such as forming metals or superconducting nanowires on nanotube templates.[9] In those cases, the bonding between CNs and metals depends on the detailed contact conditions, and careful studies are required to shed light into these issues.

Recent experiments[9,10] showed that "magnetic CNs" can be successfully prepared. Theoretical[11–14] works related to magnetic transition metals interacting with CNs have been reported in the literature. Andriotis et al.[11] indicated from their calculations on the system of Ni and CN that contact resistance in CN sensitively depends on the bonding configurations of transition metal atoms on the nanotubes. Menon et al.[14] used tight-binding molecular dynamics to study the interaction of Ni with a CN and found that the interaction depends on the tube curvature. The tight-binding methods, however, are semiempirical, and the results depend on the chosen values of the parameters, which are obtained from either experiment or high-level calculations. Fargan et al.[15] investigated the interaction of an iron atom with a single-wall carbon nanotube and found that the total magnetization depends on the confinement (i.e., whether the iron atom is inside or outside the CN). On the other hand, in a broader study of Fe−carbon nanotube systems, we find that their electronic and magnetic properties depends not only the confinement but also on the specific locations of Fe atoms inside as well as outside the nanotube.

In the present work, the structural, electronic, and magnetic properties of a system of carbon nanotubes adsorbed with Fe atoms are systematically investigated using Car−Parrinello[16,17] molecular dynamics combined with ultrasoft pseudopotentials.[18] We study the Fe−CN interactions with various configurations of a single Fe atom and of Fe clusters inside and outside carbon nanotubes of various sizes. The effects of curvature and confinement are also considered by comparing the results of a carbon nanotube containing Fe atoms with those of Fe atoms adsorbed on a sheet of graphite (graphene). We find that the presence of adsorbed Fe atoms inside or outside tubes also results in stabilized Fe−CN systems. The electronic properties and magnetic moments are found to depend on the specific

* To whom correspondence should be addressed. E-mail: mrobert@rice.edu (M.R.).
[†] Department of Chemical and Biomolecular Engineering, Rice University.
[‡] Chemistry Department and The Princeton Institute for the Science and Technology of Materials (PRISM), Princeton University.
[§] Rice Quantum Institute, Rice University.
[||] The Richard E. Smalley Institute for Nanoscale Science and Technology, Rice University.

10.1021/jp0761968 CCC: $40.75
Published on Web 05/03/2008

location of the Fe atom(s) relative to the carbon surface, and the FeaCNs can be turned into ferromagnetic materials.

The paper is organized as follows. In section I, we discuss the computation details and structural relaxation. Section II covers the structural stabilities including binding, distortion, and absorption energies. The electronic and magnetic properties of the optimized structures are discussed in section III. In sections IV and V the effects of confinement and curvature on electronic and magnetic properties, and the magnetic properties of Fe clusters inside the CNs are respectively presented. In the present study, CNs will always be assumed to be single-wall CNs, and they will most often be denoted for simplicity by CN.

Structural Optimization

The systems of iron atoms and carbon nanotubes (Fe−CN) as well as graphite (Fe−graphite) are investigated by using Car−Parrinello molecular dynamics.[16] The CP90 package[17] is used, in which density functional theory (DFT) within a plane-wave pseudopotential framework is adopted. The Perdew−Burke−Ernzerhof (PBE)-type generalized gradient approximation[19] (GGA) is employed for the exchange and correlation functional. A supercell approach is adopted so that sampling the k space at the Γ point can produce the system's electronic structure to a reliable extent. Vanderbilt ultrasoft pseudopotentials for Fe and C atoms are utilized, with a kinetic energy cutoff of 25 Rydbergs (Ry) for the wave functions and a charge density cutoff of 250 Ry. This choice of energy cutoff is based on converging values of the binding energy, bond length, and vibration frequency of Fe_2 dimer for various cutoff energies. The bond length and vibration energy are found to be 2.00 Å and 308 cm^{-1}, which agree well with experimental values (2.02 Å and 300 cm^{-1}). The converged binding energy is found to be 2.43 eV. For the pseudopotential of C, consistence with the experimental data for the values of bond lengths of benzene is also found. The geometry optimization, total magnetic moment, Fermi energy, and energy band gap of the Fe−CN systems are determined by allowing all the atoms to relax and the spins to polarize.

Two carbon nanotubes of different diameters, CN(8,0) and CN(11,0), are considered as well as a graphene sheet that can be regarded as a CN without curvature. All the calculations for a pure CN and combined Fe−CN are performed in an orthorhombic supercell with periodic boundary conditions. The sizes of the corresponding supercells of CN(8,0), CN(11,0), and graphite are 11.64 Å x 11.64 Å x 8.73 Å, 14.82 Å x 14.82 Å x 8.73 Å, and 12.60 Å x 13.10 Å x 11.64 Å, respectively. In all cases, the dimensions of the supercells are large enough that the interactions between the periodic images of Fe atoms become negligible.

CN (8,0) has a zigzag pattern and is semiconducting. For such a pure nanotube, we obtain an energy band gap of 0.49 eV and a diameter of 6.26 Å, which are consistent with those found by Fagan et al.[15] (energy band gap of 0.46 eV and tube diameter of 6.26 Å). Eight adsorption scenarios are investigated (see Figures 1 and 2). Among them, an iron atom is adsorbed inside the tube in four cases: (i) the Fe atom is above the center of a hexagon of six carbons, at a hole position (IH); (ii) the Fe atom is above the center of a symmetric C−C bond parallel to the axis of the tube (IBs); (iii) the Fe atom is above the center of an asymmetric C−C bond along the radial direction of the tube (IBa); (iv) the Fe atom is right above a carbon atom, at a top position (IT). Similarly, a Fe atom can be absorbed outside the tube in four situations: OH (Fe is at a hole position outside the tube), OBs (a symmetric bond position outside the tube),

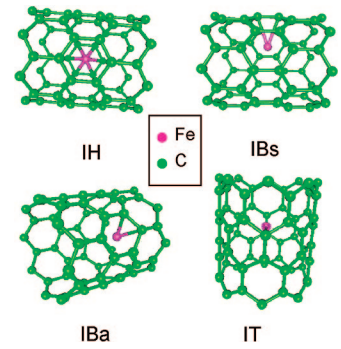

Figure 1. Four positions of the Fe atom inside the tube: IH (the Fe atom is above the center of a hexagon of six carbons), IBs (the Fe atom is above the center of the C−C bond parallel to the axis of the tube, symmetric bond), IBa (the Fe atom is above the center of the C−C bond along the radial direction of the tube, asymmetric bond), and IT (the Fe atom is on top of a carbon atom).

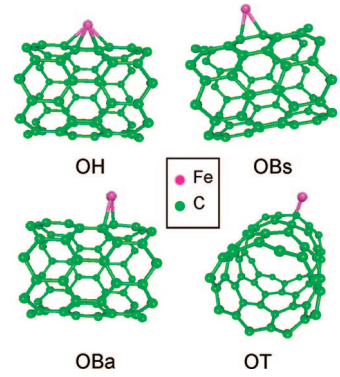

Figure 2. Four positions of the Fe atom outside the tube: OH (the Fe atom is above the center of a hexagon of six carbons), OBs (the Fe atom is above the center of the C−C bond parallel to the axis of the tube), OBa (the Fe atom is above the center of the C−C bond along the radial direction of the tube), and OT (the Fe atom is on top of a carbon atom).

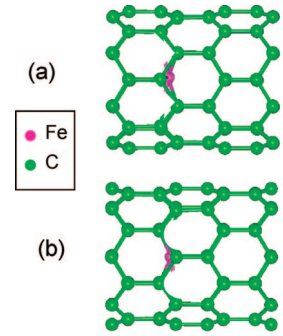

Figure 3. Positions of the Fe atom after relaxation for (a) IBa structure and (b) IT structure.

OBa (an asymmetric bond position outside the tube), and OT (a top position outside the tube) (see Figure 2).

After relaxation, except for the cases of IBa and IT, the relative positions of the Fe atom remains the same as described above, and only the distance of the Fe atom from the tube surface changes. That is, e.g., for the IH case, the Fe still stays above the center of the hexagon of six carbon atoms. For the case of IBa, the Fe atom however no longer stays directly above the center of the C−C bond along the tube radial direction but rather slightly moves away from it (see Figure 3a). Because of the curvature of the tube, the C−C bonds are not pure π bonds but have partial sp^3 character. Because of this pyramidalization, the p_z orbitals of the carbons are more densely packed inside

TABLE 1: C−Fe and Fe−Fe Bond Lengths (Å) for Fe−CN(8,0) Systems

		Fe−C_1	Fe−C_4	Fe−C_2	Fe−C_3	Fe−C_5	Fe−C_6
				inside[a]			
IBs	present			2.09	2.09		
IBs	ref 15			2.00	2.00		
IBa	present	2.03		2.06			2.09
IH	present	2.18	2.18	2.04	2.04	2.04	2.04
IH	ref 15	2.20	2.20	2.10	2.10	2.10	2.10
IT	present	2.02		2.09			2.09
				outside[a]			
OBs	present			2.07	2.07		
OBs	ref 15			2.10	2.10		
OBa	present	2.09[b]		2.13[b]			
OH	present	2.06	2.06	2.20	2.20	2.20	2.20
OH	ref 15	2.10	2.10	2.40	2.40	2.40	2.40
OT	present	2.00					

[a] The six C atoms of the hexagonal ring are labeled in a clockwise direction from 1 (C_1) to 6 (C_6) so that the C_2−C_3 and C_5−C_6 bonds are parallel to the axis of the CN. [b] Only the distances from the Fe atom to the nearest and next nearest neighbor C atom are listed here.

the tube, making the electron density of the convex side slightly differ from that of the concave side. As a result of this confinement inside the tube, the Fe atom tends to move away from the middle of the C−C bond to reduce the electron repulsion. In its new position, the Fe atom is found to bind with the three nearest-neighbor carbons (see Figure 3a). Similar explanations apply to the case of IT, where the three C−C bonds neighboring the Fe atom are not equivalent (one along the axial direction and the other two along the radial direction). The Fe atom moves away from the top position (see Figure 3b) to avoid the electron repulsion from the two next nearest-neighbor C−C bonds along the radial direction. The Fe atom forms bonds with the three nearest carbon atoms, as observed for the case of IT. On the other hand, for the cases of OT and OBa, since on the concave surface the confinement is released, the effect of electron repulsion as described above is much reduced. Consequently, the Fe atom is not pushed away but remains above the top for the OT case and about the middle of the C−C bond along the radial direction for OBa. The difference in the most stable configuration (IT and IBa for the inside case and OH for the outside case) clearly results from the confinement effect. It is however noted that, as the degree of curvature decreases, this difference no longer holds (see the section Effects of Varying Curvature).

To investigate the effect of confinement caused by the curvature (inside vs outside), the Fe−C bond lengths for the cases of Fe inside and outside the CN are compared. Table 1 lists the optimized Fe−C bond lengths for the 8 scenarios mentioned above. As seen from Table 1, while the difference in bond length between IBs and OBs is small, there is a distinct difference in the bond lengths in IH and OH (see Figure 4). For the cases of IBs and OBs, because the C−C bond facing the Fe atom is parallel to the tube axis, the bonding of the Fe atom with these two carbons is not affected by the curvature of the tube surface. On the other hand, the large difference in bond length (in the IH and OH) results from the curvature of the tube surface (convex vs concave). In the IH configuration, the Fe−C_1 and Fe−C_4 bonds are (∼2.18 Å) longer than the Fe−C_2, Fe−C_3, Fe−C_5, and Fe−C_6 bonds (∼2.04 Å). In contrast, in the OH configuration, the Fe−C_1 and Fe−C_4 bonds are shorter than the Fe−C_2, Fe−C_3, Fe−C_5, and Fe−C_6 bonds. Consistent with these bond lengths the density profiles of the IH and OH (not shown) also reveal stronger interactions of the Fe atom with the atoms C_1 and C_4 for OH and C_2, C_3, C_4, and C_5 for IH configuration. These differences obviously originate from the curvature of the tube.

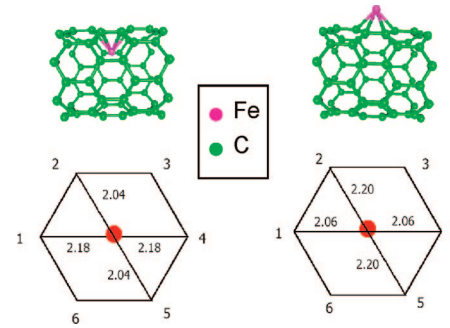

Figure 4. The difference in bond lengths of structures IH and OH is a consequence of the confinement effect (see text).

TABLE 2: Binding Energy (eV), Total Magnetic Moments (μB), Charge Transfer of Various Configurations of One Fe Atom inside and outside a CN(8,0), Distrortion Energy (E_{dis}) and Absorption Energy (E_{abs})[a]

position	E_b (eV)	E_{dist} (eV)	E_{abs} (eV)	M (μ_B)	charge transfer
			inside		
IH	−1.08	0.23	−1.31	2	0.426
IT	−1.19	0.39	−1.58	4	0.501
Ibs	−0.92	0.33	−1.25	4	0.476
Iba	−1.19	0.34	−1.53	4	0.515
			outside		
OH	−1.41	0.12	−1.53	2	0.38
OT	−1.04	0.2	−1.24	4	0.255
Obs	−1.06	0.17	−1.23	4	0.288
Oba	−0.98	0.14	−1.12	4	0.217

[a] The symbols IH, IBs, IBa, and IT denote the Fe atom being at the hole, symmetric bond, asymmetric bond, and top position inside the tube, respectively. Similarly, there are also 4 positions of Fe atom outside the tube: OH, OBs, OBa, and OT (the letter I replaced by O means outside the nanotube).

Stability: Binding, Distortion, and Absorption Energies

To understand the effect of curvature on the stability of the eight configurations considered in this work, the binding energy, distortion energy, and absorption energy are computed and listed in Table 2. The binding energy E_b is defined as the energy difference between the energy of the combined Fe−CN system and that of the pure CN and of an isolated Fe atom: $E_b = E(\text{Fe−CN}) - E(\text{CN}) - E(\text{Fe})$. The binding energy is also a measure of how stable a configuration is. As seen from Table 2, among the various positions of the Fe atom outside the tube, the most stable structure is the OH with a binding energy of −1.41 eV, consistent with the finding of Fagan et al.[15] On the other hand, for the cases of the Fe atom inside the tube, the two structures IT and IBa have similar binding energy (E_b = −1.19 eV) and are the most stable. As mentioned in the previous section, for the cases of IT and IBa, after relaxation the Fe atom no longer stays at its initial position but slightly moves away to a new position (see parts a and b of Figure 3) to avoid electron repulsion. The configurations corresponding to these new positions of the Fe atoms for these two cases are energy equivalent.

Comparison of the binding energy for the cases of Fe inside and outside the tube reveals that the OH configuration is the most stable structure. This does not mean however that CNs cannot be filled with Fe, since all eight configurations with the Fe atom outside and inside a CN are stable, and the differences

in energy between the inside and outside configurations is small (see Table 2). This observation is supported by previous experimental studies where CNs can be filled with Fe atoms (see, e.g., Su et al. and Karmaka et al. in ref 9).

To further understand the interaction of the Fe atom with the CN, the binding energy is decomposed into a distortion energy, which is the energy penalty paid to distort the nanotube, and an absorption energy, which is the energy gained when the Fe atom is absorbed onto the distorted nanotube, as seen in the chemical absorption of aromatic molecules on Pt(111).[20] The absorption energy is therefore determined as the difference of the binding energy (negative quantity) and the distortion energy (see Table 2). The distortion energy is defined as the difference between the energy of the isolated molecule and that of the distorted molecule when it is absorbed. As seen from Table 2, the distortion caused by absorption of a Fe inside the tube is more pronounced than that of a Fe outside the tube due to the confinement inside the tube. Inside the CN, while the distortion energy is the lowest when the Fe atom is at the hole position, the absorption energy is higher when the Fe atom is at the top and bond positions. This is in accord with intuition, since at the hole position the effect of electron repulsion should be smaller than at the top and bond positions.

The dependence of absorption energy on the location of the Fe atom can be further analyzed by observing the electron density difference $\Delta\rho$ between the combined Fe−CN system and the Fe atom and CN (see Figures 5 and 6). In the case of an iron atom inside the tube, more charge delocalization is observed (from the nearest neighbor to farther C atoms) for the cases IT and IBa than for the cases of IH and IBs. Such a charge delocalization serves to stabilize the structures IT and IBa, since it helps to relieve electron repulsion due to the confinement inside the tube. This delocalization accounts for the larger negative of absorption energy of IT and IBa than those of the structures IH and IBs. For the case of the Fe atom outside the CN, the charge is more localized since less distortion occurs. The highest negative value of the binding energy of the OH structure compared to those of other structures can be explained by the fact that it has the high absorption energy but the least distortion energy.

By comparison of the electron profiles of the Fe atom inside and outside the tube, two striking features are observed. First, while the electron density around the Fe atom is found to increase at some parts and decrease at other parts (negative (light blue) and positive (dark blue) $\Delta\rho$), the electron density in the vicinity of the carbon nanotube facing directly the Fe atom (i.e., the convex side of the IH and the concave side of the OH) is found to decrease, and the electron density of the other side (i.e., the concave side of the IH and convex side of the OH) is found to increase upon the absorption of an iron atom (see the side views of Figures 5and 6). Second, the charge density delocalizes in the cases of the Fe atom inside the tube and localizes for the case of the Fe atom outside the tube. This difference results from the confinement inside the tube.

Electronic and Magnetic Properties

In all configurations considered, there is a net charge transfer from the Fe atom to the CN. The amount of charge transfer is estimated by projections of molecular orbitals onto the orthonormalized atomic pseudo-orbitals[21] and via Lowdin population analysis.[22] It is noted that, because of the difficulty of partitioning charge between systems with mutually overlapping charge density distributions, the calculated charge transfer is mainly indicative, and in particular the trends predicted are informative.

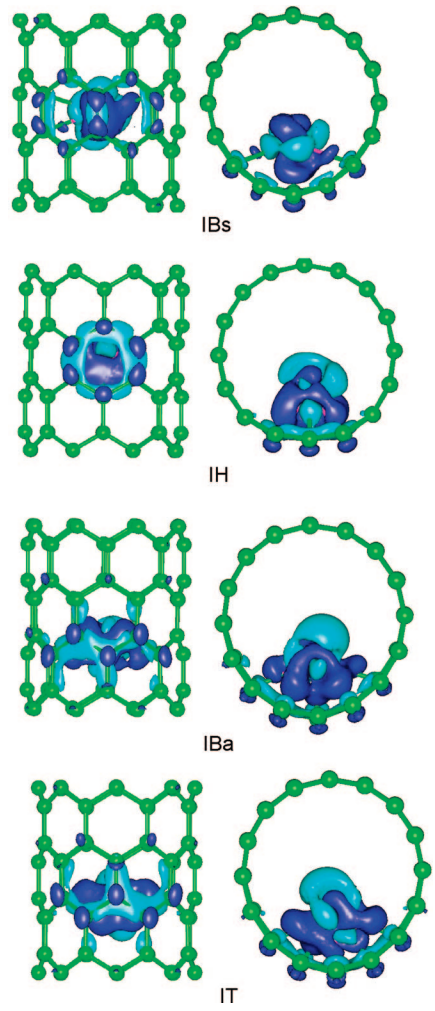

Figure 5. Difference in electron density $\Delta\rho$ between the combined system Fe−CN and the isolated Fe and CN as they are in their distorted configurations; the plot is for the case of the Fe atom inside the tube: IBs, IBa, IH, IT. The negative values of $\Delta\rho$ are plotted in light blue, and the positive values of $\Delta\rho$ are plotted in dark blue. The left and right columns correspond to the top and side views, respectively.

In the cases of an iron atom inside a carbon nanotube, the amount of charge transfer is found to be higher for IT, IBa, and IBs than for IH (see Table 2). This observation is consistent with the fact that more C atoms are involved in bonding with the Fe atom for the three structures IT, IBa, and IBs. On the other hand, in the case of the Fe atom outside the tube, the structures OH and Obs have more charge transfer than other remaining structures because more C atoms are involved in bonding with the Fe atom for these two structures (OH and Obs) than for the other two structures (OT and OBa).

Table 2 also reveals that more charges are transferred from the Fe atom to the CN for the case inside the tube than for the case outside the tube. This difference can be understood by the analysis of the density difference $\Delta\rho$ (see also Figures 5 and 6). The density profiles show that while for the outside cases the charges are localized on only a few nearest-neighbor C atoms, for the inside cases the charges delocalize to farther C atoms (including nearest-neighbor and next and next-nearest-neighbor C atoms). Bonding between Fe and C atoms involves more C atoms for the inside than the outside cases as a result of the confinement (convex vs concave). These results are consistent with intuition: because of the confined geometry of the inside of the tube, compared to the outside, a larger number of neighboring C atoms are at close distances from the Fe atom

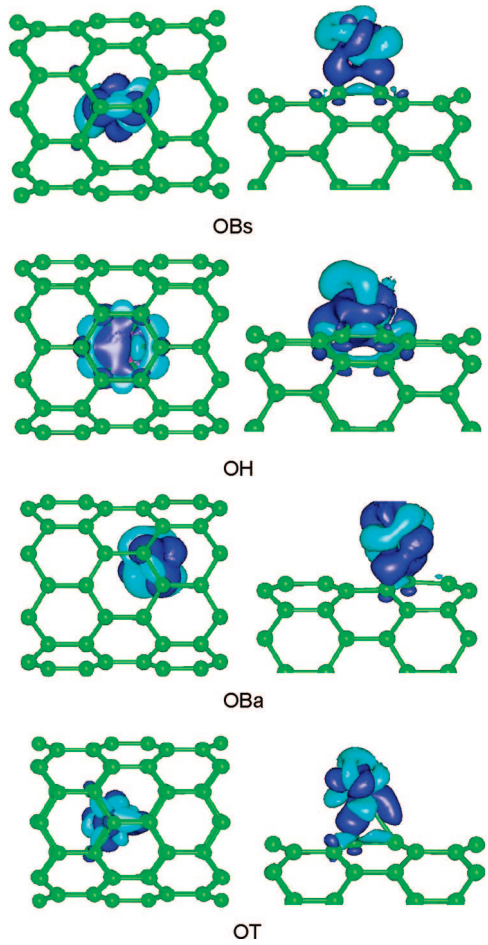

Figure 6. Difference in electron density $\Delta\rho$ between the combined system Fe−CN and the isolated Fe and CN as they are in their distorted configurations; the plot is for the case the Fe atom outside the tube: OBs, OBa, OH, OT. The density is viewed from the outside of the CN wall opposite to the wall having the absorbed Fe atom. The left and right columns correspond to the top and side views, respectively. The CNs in the right column are cut for clearer views.

TABLE 3: Fermi Energy (E_f) and Band Gap Energy (E_g) for Various Configurations of One Fe Atom inside and outside a CN(8,0)[a]

configuration	E_f (eV)	E_g (eV)	ΔE_g (eV)	ΔE_f (eV)
pureCN	−1.68	0.49		
		Fe–CN		
IH	−1.46	0.21	0.28	0.23
IBs	−1.42	0.24	0.25	0.27
IBa	−1.52	0.38	0.11	0.16
IT	−1.51	0.38	0.11	0.17
OH	−1.35	0.32	0.17	0.33
OBs	−1.42	0.22	0.27	0.26
OBa	−1.41	0.09	0.40	0.26
OT	−1.43	0.22	0.26	0.25

[a] ΔE_f is the difference in Fermi energy between the combined system Fe−CN and pure CN. ΔE_g is the difference in band gap energy between the combined system Fe−CN and pure CN. All quantities are in angstroms.

and thus expected to participate in bonding with the Fe atom. Figure 5 shows a slight distortion of the tube due to the Fe atom forming bonds with more atoms.

As a result of charge transfer, changes in energy band gap and Fermi energy are also expected. Table 3 summarizes the Fermi energy and band gap values of the combined Fe−CN systems as well as those of the pure CN. In Table 3, E_F and E_g are the Fermi energy and band gap, respectively. Comparison between the Fe−CN system and the pure CN is made by computing the difference in Fermi energy ΔE_F and band gap ΔE_g. For all cases, absorption of the Fe atom inside or outside the CN results in a decrease in band gap and an increase in Fermi energy, because there is a net charge transfer from the Fe atom to the CN, and the introduction of localized state(s) with either d or s character by the Fe atom. It is interesting to point out that the decrease in the band gap for the case of OBa is so large that the combined system Fe−CN becomes semimetallic (very small band gap $E_g = 0.09$ eV), while in other cases the Fe−CN systems still behave as semiconductors. This means that the electronic properties can be controlled by doping the Fe atom at different sites on the CN.

The total magnetic moments M for the various Fe−CN structures achieve nonzero finite values. Most of the structures listed in Table 2 give a total magnetic moment M of 4.00 Bohr magnetons (μ_B), except for the cases of IH and OH, for which the total magnetic moments are 2.00 μ_B. In other words, the present results show that the values of the total magnetic moments depend on the specific positions of Fe atom relative to the CN wall regardless CN diameter and the side of which the Fe atom is absorbed on. The dependence of M on the specific positions of Fe atom arises from the fact that the symmetry and arrangement of the surrounding C atoms are different in each case, ie., whether the Fe atom is at a hole, top, or bond position. Furthermore, at different positions of the Fe atom, the amount of charge transferred and extent of delocalization are different and thus result in a different magnetic moment. It is noted that compared to the total magnetic moment of a single Fe atom in vacuum (4.0 μ_B), the reduction of the total magnetic moment of the Fe-CN systems is observed only when the Fe atom is at the hole (IH and OH) positions.

Effects of Various Curvatures

To further investigate the effects varying curvatures (and thus size effects), the interaction of an iron atom with CN systems with larger curvatures than CN(8,0) are considered. In the present work, a CN of larger diameter (11,0) and a graphite sheet corresponding to zero curvature (or infinite diameter) are studied.

Systems of a Carbon Nanotube (11,0) and One Fe Atom. CN (11,0) is a zigzag and semiconducting nanotube with a diameter of 8.61 Å. Similar to the case of one Fe atom inside the CN(8,0), four different sites of the Fe atom are considered: hole (IH), top (IT), symmetric bond (IBs), and asymmetric bond (IBa). The binding energy, total magnetic moment, and bond length for the optimized configurations are summarized in Table 4. In contrast to the case of the smaller diameter tube CN(8,0), for the case of Fe inside the tube, the most stable configuration is the IH. This difference obviously results from the relief of the confinement associated with a decrease in curvature. Similar to the case of CN(8,0), a reduction of the total magnetic moment occurs compared to the total magnetic moment of a single Fe atom in vacuum when the Fe atom is at the hole position (IH).

Systems of Graphene and One Fe Atom. A sheet of graphite (graphene) corresponds to the extreme case of a carbon nanotube of infinite diameter (zero curvature). The interaction of an iron atom with graphene is also investigated for the three different positions of the Fe atom: hole (HG), bond (BG), and top (TG) positions. The binding energy, total magnetic moment, and charge transfer are given in Table 5. The most stable configuration is the one with the Fe atom at the hole position, which is similar to the case of the large tube CN(11,0). The binding

TABLE 4: Binding Energy (eV), Total Magnetic Moments (in μ_B), and Bond Lengths of Various Configurations of One Fe Atom inside a CN(11,0)

			bond length					
position	E_b (eV)	M (μ_B)	Fe−C_1	Fe−C_4	Fe−C_2	Fe−C_3	Fe−C_5	Fe−C_6
IBs	−0.65	4	2.16	2.16				
IBa	−0.52	4	2.18		2.18			
IH	−1.06	2	2.16	2.16	2.04	2.04	2.04	2.04
IT	−0.36	4	2.18					

TABLE 5: Binding Energy (E_b), Total Magnetic Moments (M, in μ_B), Charge Transfer, Average Distance of the Fe Atom from Graphene Surface (z), and C−Fe Bond Length (D_{C-Fe}) of Various Configurations of One Fe Atom on a Graphite Sheet (Graphene)

position		E_b (eV)	M (μ_B)	charge transfer	z (Å)	D_{C-Fe} (Å)
hole	present	−0.98	2	0.370	1.51	2.11
hole	ref 23	−2.00	2		1.52	
bond		−0.35	4	0.164	2.05	2.18
top		−0.35	4	0.135	2.09	2.09

energies and the amount of charge transfer for the case of Fe−graphene, however, are smaller than for the case of Fe−CN(8,0). Clearly, the presence of curvature in the CN leads to a stronger bonding between the Fe atoms with CN than with graphene.

For the HG configuration, the present binding energy is about half of that found in the study of Duffy et al.[23] The discrepancy results from the different methods used in determining the exchange-correlation energy. While in ref 23, the LDA is used, which is well-known for overbinding effects, in this study the GGA is used, which is known to correct this problem.[24]

The effects of varying curvatures on the interaction of the Fe atoms with CN's and graphene are summarized in Figure 7. For the case of Fe inside the tube, the most stable structure changes from the bond/top for CN(8,0) to the hole position for CN(11,0) and graphene. In other words, as the tube curvature decreases (and the tube diameter increases), the most stable structure varies. At a small enough curvature (e.g., equal to or smaller than that of CN(11,0) in this work), the most stable configuration is the hole position. On the other hand, for the case the Fe atom outside the tube, the results of our calculations (not shown here) show that the most stable structure is the hole position for all CN diameters considered in this work. This similarity in the most stable configuration being the hole position (see Figure 7) indicates that curvature effects are most pronounced for the small diameter carbon nanotubes, in accord with intuition.

The effects of various curvatures on the most stable configuration shown in Figure 7 and the binding energy can also be further understood by analyzing the highest-occupied molecular orbital (HOMO) densities of three Fe−CN systems with different degrees of curvature. Figure 8 illustrates three different systems with decreasing curvature: Fe−CN(8,0), Fe−CN(11,0), and Fe−graphene, where the Fe atom is at the hole position and inside the tube. As the curvature increases, the degree of charge depletion at the C atoms surrounding the Fe atom decreases. While charge depletion is observed to occur at all six carbon atoms of the hexagon facing the Fe atom for the graphene case, it takes place only at four carbon atoms for the CN cases. Furthermore, delocalization is observed at the remaining two C atoms with their next neighboring C atoms along the CN axis, whereas such delocalization is absent in the graphene case. This difference explains why the binding energy is higher for CN than for graphene.

Comparison of the HOMO densities of the IH configurations for the Fe−CN(8,0) and Fe−CN(11,0) systems shows that the upper and lower C−C bonds (marked with the red arrows in Figure 8a) of the hexagon facing the Fe atom have more sp^3 character in CN(8,0) than those in CN(11,0) (see Figure 8b). This obviously results from the higher degree of curvature in CN(8,0). On the other hand, the HOMO densities of the OH configurations for Fe−CN(11,0) and Fe−CN(8,0) reveal that the delocalization at the C atoms neighboring the Fe atom is similar to that shown in Figure 8b. In other words, while for a CN with a high degree of curvature (such as CN(8,0)) delocalization at C atoms neighboring to the Fe atom for the IH differs from that of the OH, for a CN with a smaller curvature (such as CN(11,0)), delocalization is observed to be similar for the IH and OH cases. This difference is due to the larger confinement caused by the larger curvature in the smaller tube, explaining the changes in the most stable configuration as the

The most stable configuration			
System	CN(8,0)	CN(11,0)	graphene
D(Å)	6.3	8.6	∞
Inside	bond/top	hole	hole
Outside	hole	hole	hole

Figure 7. Effects of curvature: the most stable configuration changes as the curvature varies.

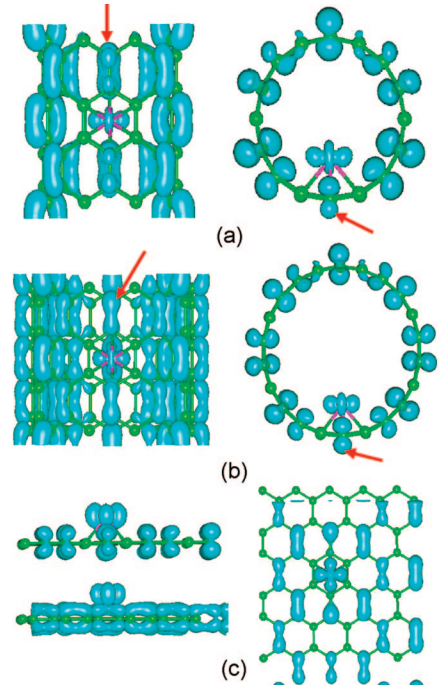

Figure 8. HOMO densities of three systems (a) Fe−CN(8,0), (b) Fe−CN(11,0), and (c) Fe−graphene, where the Fe atom is at the hole position. The left and right columns are the side and top views, respectively. For the case of graphene, two side views (viewed from the x and y directions) are shown.

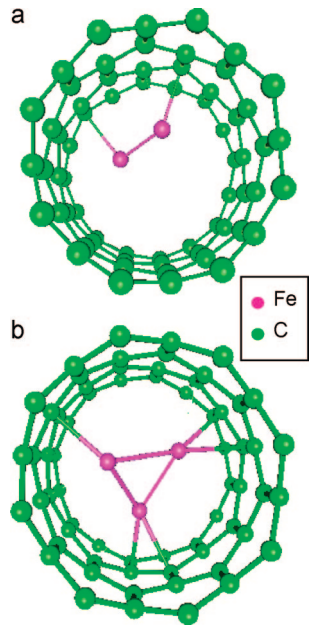

Figure 9. Optimized structures of a (a) dimer Fe_2 and a trimer (b) Fe_3 inside a CN(8,0).

TABLE 6: Binding Energy per Fe Atom, Total Magnetic Moment per Atom, and Fe−Fe Bond Lengths for Clusters (Fe_2 and Fe_3) for Fe Atoms inside a CN(8,0) and in a Vacuum

Fe cluster-CN	E_b (eV)/atom	M (μ_B)/atom	Fe−Fe (Å)	notes
		Fe_2−CN		
bond−top	−1.83	3.00	2.29	
hole−hole	−1.48	3.00	2.28	
hole−bond[a]	−1.46	4.00	2.27	
hole−bond[b]	−1.81	4.00	2.22	
bond−bond[a]	−1.91	4.00	2.28	
top−top	−1.90	4.00	2.29	
Fe_3−CN				
	−2.15	0.67	2.21, 2.41, 2.41	
		Fe cluster		
Fe_2	−1.22	3.00	2.00	
	−3.17	3.00	2.06	ref 26
	−1.15 ± 0.09[c]	3.00	2.02	refs 27, 28
Fe_3	−1.79	12.00	2.30, 2.30, 2.30	
	−1.70	10.00	2.29, 2.29, 2.30	
	−1.55	8.00	2.17, 2.17, 2.16	
	−1.46	4.05	2.12, 2.41, 2.41	

[a] Symmetric bond. [b] Asymmetric bond. [c] The experimental data are also given in ref 26.

curvature decreases from CN(8,0) to CN(11,0) and to graphene (see Figure 7).

Systems of a Carbon Nanotube (8,0) and Dimer Fe_2 and Trimer Fe_3

Similar to the case of one Fe atom inside a CN, clusters of Fe atoms inside a CN are also studied. Parts a and b of Figure 9 show the optimized configurations of a dimer Fe_2 and a trimer Fe_3 inside a CN(8,0). Table 6 lists the binding energy, total magnetic moment, and the Fe−Fe and Fe−C bond lengths for a dimmer Fe_2 and a trimer Fe_3 in a vacuum and inside a CN(8,0). The binding energy is calculated by using the following formula: $E_b = E_{tot} - E_{CN} - 3E_{Fe}$, where E_{tot} is the total energy of the system Fe−CN, E_{CN} is the energy of the CN, and E_{Fe} is the energy of an isolate Fe atom.

For the case of Fe_2, various initial configurations are considered: hole−hole, bond−bond, top−top, hole−bond (C−C bonds along the nanotube axis and in radial direction are considered). These configurations are chosen such that bonding between Fe and Fe is still maintained. The bond−bond configuration is found to be the most stable configuration. Compared to the case of a dimer Fe_2 in vacuum, the interaction of Fe atoms with the CN enhances the total magnetic moments of the system Fe_2−CN, and the Fe−Fe bond length is found to increase by 11−14.5%. Furthermore, since the binding energy between Fe and Fe atoms is larger than that between a Fe atom and CN, it is expected that inside large nanotubes Fe atoms will tend to form clusters. These results are consistent with experimental studies showing Fe clusters are formed inside[25] and outside[9] CNs. In making various metallic nanowires formed on carbon nanotubes templates, Dai et al.[9] found that Ti and Ni form continuous nanowires, while Fe can only form large discontinuous clusters inside and outside the tubes.

For the case of Fe_3 inside a CN, several stable configurations with different total magnetic moments can be found, depending on the position of each Fe atom inside the tube. The most stable configuration is found by performing simulation at high temperature, followed by gradually cooling the system to 0 K. Note that longer tube length is used (the unit cell contains 96C) for this case to make the interaction between periodic images negligible. The Fe atoms inside the CN are found to form a cluster (triangular trimer), and bonding of Fe atoms with CN lead to significant decreases in total magnetic moments compared to those of the case of a trimer Fe_3 in vacuum. In this stable structure, two of the three Fe atoms are found to be close to the position similar to the case of IBa. The remaining Fe atom is close to the hole position. Table 6 lists the total magnetic moments and binding energy for this Fe_3−CN structure and three different configurations of Fe_3 clusters in vacuum for the purpose of comparison with the Fe_3−CN system. Similar to the case of Fe_2, inside a CN, the Fe−Fe bond length also increases due to the interaction between Fe atoms and the CN.

It is noted from Table 6 that the Fe_3 cluster has a much smaller magnetic moment when adsorbed into a CN if compared to vacuum. For Fe_3 cluster in vacuum, while those configurations having high magnetic moments are equilateral or closely equilateral (see the first three lines for Fe_3 in vacuum in Table 6), the isosceles configuration has much lower magnetic moment (this also applies to other regular triangular configurations, which are not listed in Table 6). In the highest symmetry system (equilateral), the number of degenerate energy bands is also highest, and thus the high spin state is preferred. As the system is slightly distorted and the system symmetry is reduced, the degeneracy is lifted, whose degree of lifting depends on how large the distortion or perturbation is. If the distortion is large enough, a strong degeneracy lifting occurs. Consequently, the lower spin state is preferred. For the Fe_3 cluster inside a CN, the interactions of the Fe atoms with the C atoms of the CN make the regular triangle configuration the preferred configuration. Therefore, a much smaller magnetic moment is observed.

Conclusions

Systems of CNs of various diameters and graphene with absorbing Fe atoms are investigated by using the Car−Parrinello molecular dynamics method. In contrast to the case of pure CNs, whose total spin magnetic moment is zero, the present results show that the total spin magnetic moments of these systems attain nonzero values. For the case of one Fe atom inside a CN, while the most stable configuration is dictated by the

confinement effect, the magnitude of the total magnetic moment is found to depend on the specific location of the Fe atom. The Fe atoms (dimer and trimer) inside a CN are found to couple ferromagnetically, which is very promising for studying quasi-one-dimensional ferromagnetic CN-based materials for applications such as spintronics (e.g., magnetic tunneling junction). Furthermore, by stacking ferromagnetic CNs together, two-dimensional and three-dimensional ferromagnetic or antiferromagnetic CNs can be made, depending on whether the intertube couplings are ferromagnetic or antiferromagnetic.

Acknowledgment. We thank Prof. Filippo de Angelis for providing us with the Fe and C pseudopotentials, and we thank the referee for his constructive comments. At Rice University, this work was supported by the Welch Foundation (Houston, TX). At Princeton University, this work was supported by the National Science Foundation (Grant No. CHE-0121432). The computation was performed on the Keck Computational Center in The Princeton Institute for the Science and Technology of Materials (PRISM) of Princeton University.

References and Notes

(1) (a) Dressehaus, M. S.; Dressehaus, G.; Avouris, P. *Carbon Nanotubes*; Springer: Berlin, 2001. (b) Dai, H. *Surf. Sci.* **2002**, *500*, 218. (c) Thostenson, E. T.; Ren, Z.; Chou, T. W. *Compos. Sci. Technol.* **2001**, *61*, 1899. (d) Collins, G. P.; Avouris, P. *Sci. Am. Dec.* **2000**, 62. (e) Iijima, S. *Physica B* **2002**, *323*, 1.

(2) Thostenson, E. T.; Ren, Z. F.; Chou, T. W. *Compos. Sci. Technol.* **2001**, *61*, 1899.

(3) Vaseashta, A. *J. Mater. Sci.* **2003**, *14*, 653.

(4) (a) Fuse, T.; Moriyama, S.; Suzuki, M.; Aoyag, Y.; Ishibashi, K. *Appl. Phys. Lett.* **2003**, *83*, 3803. (b) San-Huang-Ke, N.-A.; Baranger, H. U.; Weitao, Y. *Phys. Rev. Lett.* **2003**, *91*, 116803.

(5) (a) Star, A.; Han, T. R.; Gabriel, J. C. P.; Bradley, K.; Gruner, G. *Nano Lett.* **2003**, *3*, 1421. (b) Freitag, M; Martin, Y.; Misewich, J. A.; Martel, R; Avouris, P. H. *Nano Lett.* **2003**, *3*, 1067. (c) Babic, B.; Iqbal, M.; Schonenberger, C. *Nanotechnology* **2003**, *14*, 327.

(6) Haruyama, J.; Takesue, I; Hasegawa, T. *Physica E* **2002**, *12*, 735.

(7) (a) Vo, T. T. M.; Ph.D. Thesis, Rice University, 2004. (b) Vo, T. T. M.; Lee, T.-C.; Payandeh, B.; Robert, M. Magnetic Carbon Nanotubes. *Proceedings of the First Topical Conference on Nanometer Scale Science and Engineering*; LAIChE: New York, 2001; pp 369−377.

(8) (a) Charlier, J. C.; Blase, X.; DeVita, A.; Car, R. *Appl. Phys. A* **1999**, *68*, 267. (b) Charlier, J. C.; DeVita, A.; Car, R. *Science* **1997**, *275*, 646. (c) Iijima, S.; Ichihashi, T. *Nature* **1993**, *363*, 603. (d) Bethune, D. S.; Kiang, C. H.; Devries, M. S.; Gorman, G.; Savoy, R.; Vazquez, J.; Beyers, R *Nature* **1993**, *363*, 605. (e) Thess, A.; et al. *Science* **1996**, *273*, 483. (f) Tibbetts, G. G.; Devour, M. G.; Rodda, E. J. *Carbon* **1997**, *25*, 367. (g) Bezryadin, A.; Lau, C. N.; Tinkham, M. *Nature* **2000**, *404*, 901.

(9) (a) Dai, H. J.; Wong, E. W.; Lu, Y. Z.; Fan, S. S.; Lieber, C. M. *Nature* **1995**, *375*, 769. (b) Han, W. Q.; Fan, S. S; Li, Q. Q.; Hu, Y. D. *Science* **1997**, *277*, 1287. (c) Su, Y.-C.; Hsu, W.-K. *Appl. Phys. Lett.* **2005**, *87*, 233112. (d) Guan, L.; Shi, Z.; Li, H.; Liping, G.; Zhennan, N. A. *Chem. Comm.* **2004**, 1988. (e) Karmakar, S.; Surinder; Mukadam, M. D.; Yusuf, M.; Sood, A. K. J. *Appl. Phys.* **2005**, *97*, 054306. (f) Leonhardt, A.; Ritschel, M.; Elefant, D.; Mattern, N.; Biedermann, K.; Hampel, S. J. *Appl. Phys.* **2005**, *98*, 074315.

(10) (a) Duj, E.; Meny, C.; Panissod, P.; Kintzinger, J. P.; Yao, N.; Ebbesen, T. W. *Solid State Commum.* **2000**, *114*, 543. (b) Peng, D. L.; Zhao, X.; Inoue, S.; Ando, Y.; Sumiyama, K. J. *Magn. Magn. Mater.* **2005**, *292*, 143. (c) Komogorts, S. V.; Iskhakov, R. S.; Denisova, E. A.; Balaev, A. D.; Myagkov, V. G. *Tech. Phys. Lett.* **2005**, *31*, 454.

(11) (a) Andriotis, A. N.; Menon, M.; Froudakis, G. E. *Phys. Rev. B* **2000**, *61*, R13393. (b) Andriotis, A. N.; Menon, M.; Froudakis, G. E. *Appl. Phys. Lett.* **2000**, *76*, 3890.

(12) Mao, Y.-L.; Yan, X.-H.; Xiao, Y. *Nanotechnology* **2005**, *16*, 3092.

(13) Raty, J.-Y.; Gygi, F.; Galli, G. *Phys. Rev. Lett.* **2005**, *95*, 096103.

(14) (a) Andriotis, A. N.; Menon, M.; Froudakis, G. *Phys. Rev. Lett.* **2000**, *85*, 3193. (b) Menon, M.; Andriotis, A. N.; Froudakis, G. E. *Chem. Phys. Lett.* **2000**, *320*, 425.

(15) Fargan, S. B.; Mota, R. *Phys. Rev. B* **2003**, *57*, 205414.

(16) Car, R.; Parrinello, M. *Phys. Rev. Lett.* **1985**, *55*, 2471.

(17) Baroni, S. The PWSCF code 2003, http://www.pwscf.org.

(18) Vanderbilt, D. *PRB* **1990**, *41*, 7892.

(19) Perdew, J. P.; Burke, K.; Ernzerhof, M. *Phys. Rev. Lett.* **1996**, *77*, 3865.

(20) Morin, C.; Simon, D.; Sautet, P. J. *Phys. Chem. B* **2004**, *108*, 12084.

(21) Sanchez-Portal, D.; Artacho, E.; Soler, J. M. *Solid State Commun.* **1995**, *95*, 685.

(22) Lowdin, P. O. *Adv. Quantum Chem.* **1970**, *5*, 185.

(23) Duffy, D. M.; Blackman, J. A. *Phys. Rev. B* **1998**, *58*, 7443.

(24) Pedew, J. P.; Chevary, J. A.; Vosko, S. H.; Jackson, K. A.; Perderson, M. A; Singh, D. J.; Fiolhais, C. *PRB* **1992**, *46*, 6671.

(25) (a) Prados, C.; Crespo, P.; Gonzalez, Z. M.; Hernando, R.; Marco, J. F.; Gancedo, R.; Grobert, N.; Terrones, N.; Walton, R. M.; Kroto, H. W. *IEEE Trans. Magn.* **2001**, *37*, 2117. (b) Liu, Z.-J. *Synth. Met.* **2002**, *128*, 191.

(26) Yanagisawa, S. J.; Tsuneda, T.; Hirao, K. *Chem. Phys.* **2000**, *112*, 545.

(27) Lin, S. S.; Kant, A. *J. Phys. Chem.* **1969**, *73*, 2450.

(28) Purdum; Montano, P. A.; Shenoy, G. K.; Morrison, T. *PRB* **1982**, *25*, 4412.

JP0761968